Attaining Hypersonic Flight with Aluminum-Based Fuel-Rich Propellant

Nikunj Rathi* and P. A. Ramakrishna†
Indian Institute of Technology-Madras, Chennai 600 036, Tamil Nadu, India

DOI: 10.2514/1.B36463

In this paper, experimental results of an aluminized fuel-rich propellant having energetics similar to boron-based fuel-rich propellant and having no residue after combustion are discussed. Using this aluminum-based fuel-rich propellant, which has higher density than the current fuels used for hypersonic flight, this paper looks at enhancing the Mach number envelope of a ramjet. Nondimensional thrust and drag calculations were carried out to identify the air–fuel ratio required for a Mach 6 flight, with different intakes accounting for different pressure recovery. Calculations were carried out with three different intakes, and it was observed that, even with the lowest pressure recovery of 9% at Mach 6, a hypersonic mission was possible. Values for various efficiencies were chosen with great care, and a perturbation analysis was carried out to make the calculations more robust. The specific impulse obtained with the aluminum-based fuel-rich propellant in ramjet mode was 515 s at a 25 km altitude. Comparison of an aluminum-based fuel-rich propellant in ramjet mode was made with a kerosene and hydrogen fueled scramjet from the specific impulse data available in the literature. The specific impulse of the aluminum-based fuel-rich propellant was nearly an order of magnitude higher as compared to a hydrogen fueled scramjet when adjusted to the density of hydrogen. Upon considering a system size, it was also shown that the aluminum-based fuel-rich propellant could meet the burn rate requirement for a Mach 6 flight.

Nomenclature

A	=	vehicle frontal area, m^2
A_i/A	=	ratio of air intake area to vehicle frontal area
a_o	=	speed of sound, m/s
c_d	=	coefficient of drag
c^*	=	characteristic exhaust velocity, m/s
g	=	acceleration due to gravity, m/s^2
$I_{\text{sp\_CEA}}$	=	specific impulse from NASA SP273, m/s
$I_{\text{sp\_ram}}$	=	ramjet specific impulse, s
M_o	=	flight Mach number
m_{Al}	=	aluminum mass fraction
m_{AP}	=	ammonium perchlorate mass fraction
m_{Binder}	=	binder mass fraction
$\dot{m}_a$	=	air mass flow rate, kg/s
γ	=	specific heat ratio
ϵ	=	air–fuel ratio
η_{C_F}	=	thrust coefficient efficiency
η_b	=	burner pressure efficiency
η_d	=	diffuser pressure efficiency
η_n	=	nozzle pressure efficiency
η_{c^*}	=	combustion or characteristic exhaust velocity efficiency
θ_b	=	ratio of chamber temperature to ambient air temperature
θ_o	=	ratio of total temperature to the static temperature for flight Mach number
v_o	=	vehicle flight velocity, m/s
v_4	=	exit velocity of gases through nozzle, m/s
ρ_p	=	ambient air density, kg/m^3
ρ	=	propellant density, kg/m^3
ρ_{Al}	=	aluminum density, kg/m^3
ρ_{AP}	=	ammonium perchlorate density, kg/m^3
ρ_{Binder}	=	binder density, kg/m^3

Received 10 September 2016; revision received 22 November 2016; accepted for publication 28 January 2017; published online 4 May 2017.

*Ph.D. Scholar, Aerospace Department; nikunj.rathi0@gmail.com (Corresponding Author).

†Professor, Aerospace Department; parama@iitm.ac.in.

I. Introduction

HUMANS have always been in the quest to go to higher speeds. From the first rocket-powered supersonic X-15 flight in the 1960s, researchers around the world have been in pursuit of achieving hypersonic flight with airbreathing engines [1,2]. The emphasis on airbreathing engines over rockets for hypersonic flight comes from the fact that they could deliver much higher specific impulse (I_{sp}) than a rocket engine.

Airbreathing engines fall into different types, depending up on the flight Mach number. Ramjets are used up to Mach 4; beyond Mach 5, which is considered a hypersonic regime, scramjets are proposed to be used. The reason for using a scramjet over a ramjet for flight Mach numbers beyond five is because the inlet air temperatures are very high for a subsonic combustion in the case of ramjets and there will not be enough scope for adding heat. Therefore, thrust produced is limited and may not overcome the drag experienced at Mach 5 and beyond, as explained by Hill and Peterson [3].

Research on scramjets has been going on for more than 40 years. Even with a lot of effort being put in by researchers across the globe over a long period, there has been no commercial or military vehicle with a scramjet engine used anywhere in the world. There have been a few technology demonstration flights, as is evident from Table 1. The reason for this is the sheer complexity involved in scramjet design and testing, which are adequately highlighted in the literature [1–3].

Contrary to the scramjet, a ramjet is a simpler device with lots of actual systems in use all around the world [3,4]. If the flight envelope of a ramjet can be augmented to Mach 6, then an actual hypersonic vehicle is possible with much fewer complexities as compared to a scramjet. The reason to limit the Mach number to six is because the present hypersonic research pursued by various countries [1,2] is targeted toward a Mach number between five and six with a scramjet.

At higher Mach numbers the inlet air temperature is very high in a subsonic combustor (around 1500 K for Mach 6 at 25 km) and there is less scope for sensible heat addition using conventional ramjet fuel like kerosene, which has a flame temperature of around 2500 K with air. With the difference between the stagnation temperature of air and the flame temperature of kerosene being only around 1000 K, the thrust that can be generated will also be less and might not overcome the drag experienced at Mach 6. For this to be possible, one may have to look at alternate fuels other than kerosene and hydrogen because the adiabatic flame temperature with both these fuels is lower, as will be discussed later in the paper.

Table 1 Research on hypersonic vehicle in various countries

Country	Project	Remarks
Australia	HyShot	More than Mach 7 for 6 s during a test flight in 2002[a]
China	Wu-14	No data available
India	Hypersonic technology demonstrator vehicle	Ground test of scaled model[b]
	Indian space research organisation scramjet project	Ground test carried for a duration of 7 s[c]
United Kingdom	Synergetic air breathing rocket engine	Hybrid between rocket and jet engine. Heat exchanger absorbs 400 MW of heat energy and cools the rammed air. Use of hydrogen as fuel and heat exchanger-based design made vehicle size large.[d]
United States	X-30	Cancelled without flight test
	X-43	Speed more than Mach 9 in flight test[e]
	X-51 Waverider	Longest hypersonic duration of 210 s at Mach 5.1[f]
Russia	YU-71	No data available

[a]Data available online at http://www.abc.net.au/science/slab/hyshot/default.htm [retrieved 13 July 2016].
[b]Data available online at http://defenceforumindia.com/forum/threads/drdo-to-test-hypersonic-technology-demonstrator-vehicle.43102/ [retrieved 13 July 2016].
[c]Data available online at http://www.isro.gov.in/update/10-jan-2006/isro-achieves-breakthrough-supersonic-combustion-technology [retrieved 13 July 2016].
[d]Data available online at https://www.reactionengines.co.uk [retrieved 13 July 2016].
[e]Data available online at https://www.nasa.gov/missions/research/x43-main.html [retrieved 13 July 2016].
[f]Data available online at https://www.nasa.gov/topics/aeronautics/features/X-51A.html [retrieved 13 July 2016].

Metals are known to have higher equilibrium combustion temperatures than a hydrocarbon-based fuel, as shown by Kubota et al. [5]. This higher equilibrium combustion temperature could make it possible for the ramjet to be operated at a higher Mach number. Along with a higher equilibrium temperature, there is an added advantage of higher density with metals. Figure 1 is compiled based on inputs from Risha et al. [6]. Here, it compares the heat of oxidation of metals like aluminum (Al) and boron (B) with hydroxyl-terminated polybutadiene (HTPB), kerosene, and hydrogen. Among all fuels, hydrogen has the highest heat release by weight. However, due to its very low density, the volumetric heat release is lowest among all fuels. This means that, in a given volume, a very small amount of hydrogen can be stored. This is a pertinent issue because most vehicles will be limited by volume and, as a consequence, the density of the fuel plays a very crucial role. Among the typically used metal fuels, boron has the highest gravimetric and volumetric heat of oxidation. However, it has certain disadvantages like a high melting and boiling point, as well as ignition and combustion problems at a higher boron content [7]. Also, from an economical point of view, it is around 300 times more expensive than aluminum [boron at 1300–1500 U.S. dollars (USD)/kg and aluminum at 3.2–6.35 USD/kg [8]). Thus, in the present study, aluminum is used as a metal fuel for fuel-rich propellant (FRP). Volumetric heat release (refer Fig. 1) for aluminum is twice that of HTPB, which would mean that, if one makes use of aluminum, it could result in a high-density fuel leading to a compact propulsion system.

Apart from the type of fuel, another important subsystem for a ramjet is the type of intake that is used. The ramjet systems that are in use presently have electronics in the nose portion of the vehicle, and the intakes have to be side mounted (as in the Air-Sol Moyenne Portée missile). This configuration leads to a higher coefficient of drag (≈0.6) for Mach 2, as reported by Murty and Chakraborty [9], as compared to a much lower value of around 0.14 for the nose-mounted intake, as was reported by Dutton and Goldsmith [10] in their experiments. Therefore, if an axisymmetric external compression nose cone intake (based on [10]) that has a much lower coefficient of drag is chosen, it will result in lower drag. This would mean that a kerosene ramjet can probably go to a higher Mach number than its current usage. However, a ramjet with metalized fuel can operate at an even higher Mach number with its higher combustion temperature than kerosene, as discussed earlier.

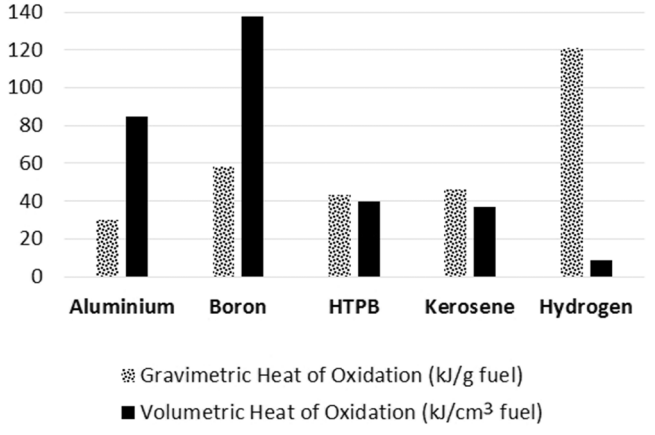

Fig. 1 Heat of oxidation for different fuels.

Previous works on boron-based fuels for ramjets have been carried out by Gany and Netzer [11] and Natan and Gany [12], but these works used them in a hybrid mode and not a fuel-rich mode. A large volume of previously published literature on FRP based on boron as the metal fuel has been carried out by Kubota et al. [5]. They had reported a maximum combustion efficiency of 91% for ramjet tests with boron-based FRP. However, the residue for their propellants in the primary chamber was not discussed. Nanda and Ramakrishna [8] prepared fuel-rich solid propellants with aluminum, ammonium perchlorate (AP), and HTPB. The propellants had comparable energetics to that of boron-based FRP, but they were extremely cost effective, as mentioned earlier. However, the residue left, or the unburned propellant, was of the order of 20–25% at the end of combustion. However, if these propellants need to find any application in an actual system, the residue needs to be below 5%.

If the residue of the FRP needs to be brought down below 5%, then one has to explore newer techniques to increase burn rates. It was observed during the preliminary experiments of this study and those by Kohga [13] that some mechanism of enhancing the burning behavior of AP or aluminum would primarily result in greater pyrolysis of ingredients, leading to lower residue due to heat release taking place very close to the burning surface. Hence, a brief review of the literature on techniques to enhance burn rates follows.

Aluminum is added as a metal fuel to increase the I_{sp} as well as the density of the propellant. The propellant burn rates can be increased by having a higher surface area of aluminum in the propellant. Nanosized aluminum has been employed in place of micrometer-sized aluminum and has been reported by Dokhan et al. [14] to result in very high burn rates in composite solid propellants. But, as the specific surface area of nanoaluminum is very large, it increases the viscosity of the propellant slurry drastically and makes it difficult to mix, as observed by Sipple et al. [15,16] and Verma and Ramakrishna [17]. Furthermore, Verma and Ramakrishna [17] proposed the use of micrometer-sized flake aluminum (pyral) with a very high surface area and a heat of combustion higher than nanosized aluminum to increase the burn rates of composite solid propellants.

Fluorination of aluminum leads to very high (volumetric and gravimetric) heat release as compared to its oxidation [15] due to thermite reactions. Therefore, when aluminum is activated with a fluorine-based compound such as polytetrafluoroethylene (PTFE), it

results in higher reactivity, and thereby increases the burn rates, as reported by Sipple et al. [16]. Similar results were reported by Gaurav and Ramakrishna [18], where mechanical activation of aluminum with PTFE resulted in a 50% higher burn rate over those obtained by Verma and Ramakrishna [17] using pyral. In this study, it is intended to make use of mechanically activated aluminum with PTFE for making fuel-rich propellants.

Ishitha and Ramakrishna [19] used activated charcoal (AC) catalyst embedding on AP to increase the burn rates of composite solid propellants. They carried out detailed studies to understand how AC embedded on AP can result in as much as 50% higher burn rates as compared to the case when they are just mixed in a solid propellant with only 1% of catalyst addition. Marothiya and Ramakrishna [20] discussed the effectiveness of embedding iron oxide (IO) on AP. They reported a 30% increase in burn rate with 1% IO using this technique as compared to just mixing. The fundamental reason why embedding catalyst (AC or IO) on AP was found to be more effective than mixing was that these catalysts act on AP alone [19,20]. In the case of just mixing these catalysts in the propellant, it gets dispersed everywhere and the interaction sites between AP and the catalyst are limited and are often hindered by the binder; whereas in the case of embedding, the catalyst is in direct contact with AP, and thus more effective.

With increased reactivity of both AP (with catalyst embedding [19,20]) and aluminum (with mechanical activation of PTFE [16,18]), they tend to burn close to the propellant surface and the heat feedback to the surface is more. This results in higher burn rates of the propellant and a reduction in the residue. Therefore, few of the techniques will be used either individually or in combination to achieve higher burn rates and lower residue that are required for a fuel-rich propellant.

To date, for hypersonic flight, a scramjet has been advocated as a preferred system. Throughout this paper, it is intended to demonstrate that, even with the use of a ramjet, it is possible to achieve hypersonic flight speeds. For this, based on the preceding discussions, a metalized fuel that results in higher-equilibrium combustion temperature than kerosene looks to be a promising choice. This metalized fuel will have the added advantage of a higher-density specific impulse because its volumetric heat release is much more than that obtained with kerosene. An axisymmetric nose cone mounted intake is seen to result in a lower coefficient of drag than a side-mounted intake. This will be incorporated in the ramjet design. The scope of this paper is to demonstrate through detailed calculations the possibility of having a ramjet capable of operating at hypersonic speeds and design an appropriate metalized fuel with burn rates sufficient to meet the thrust requirements.

II. Propellant Studies

A. Propellant Preparation

All the propellants made in the present study used AP in particle sizes of 25–45 μm. These are as shown in Table 2. In mix 1, the mechanically activated aluminum particle size was 45–63 μm and mixes 3 and 4 used mechanically activated aluminum of with particle sizes of less than 300 μm. The binder (77% HTPB, 15% Di octyl adipate, 8% IsoPhorone Di-Isocynate) was precured for 4 h to get an appropriate viscosity, such that the solids did not settle down while curing and the trapped gases could be removed from the slurry while degassing.

All the solids were crushed and sieved to their appropriate particle sizes, as indicated earlier. The procedure used for the embedding of IO and AC on AP follows the procedure described by Ishitha and Ramakrishna [19]. AP and AP embedded with IO were kept in an oven at 60°C for at least 24 h before being used so as to remove any moisture present in it. AP embedded with AC was kept in ambient conditions for around five days so that it could absorb moisture (40% by weight of AC) from the surrounding air. Once the binder precuring was done, solids were mixed one at a time in required quantities using a 0.01 g least count weighing balance.

After hand mixing all the ingredients for around 5 min, the propellant slurry was transferred to a sigma mixer where it was mixed for another 45 min. Then, the propellant slurry was taken out of the mixer and poured into a plastic pipe with one end sealed with plastic, which acted as a casing. The casing was then kept in a desiccator connected to a vacuum pump maintained at a pressure of 50 mm of mercury for 24 h to ensure that all of the trapped gases had been removed from the slurry. After this, the slurry was cured at ambient conditions for 14–15 days.

The cured propellant is then taken out of the casing and cut into samples of $5 \times 5 \times 10$ mm using a surgical knife for determining the burn rate of the propellant.

B. Experimental Setup and Procedure

A window bomb was used to measure the burn rates of the propellant in which propellant burning could be recorded through a window and burn time could be determined. A window bomb is a high-pressure vessel that can withstand pressures up to 200 bar. It has two quartz windows with diameters of 25 and 12 mm. A xenon light source was placed at the 25 mm window; and a video camera, which can record at the rate of 25 frames per second, was placed at the 12 mm window to record the propellant burning. The base plate of the window bomb consisted of a stand where the propellant sample was placed: two electrodes for ignition, and a porous plate from where the inert gas entered the chamber. At the top end of the vessel, an exhaust pipe was placed to expel the burned gases. Figure 2 show the schematic of the window bomb.

The propellant sample was coated with an inhibitor on four sides (each with an area of 10×5 mm^2) so that it burned only in one direction, i.e., from top to bottom. An inhibitor-coated propellant sample was then placed on the stand and a nichrome wire of 0.5 mm in diameter was used for ignition and connected between the two electrodes. It passed over the top surface of the propellant sample. An in-situ propellant with fine-sized AP and HTPB was applied on the top surface of the propellant sample to ensure that the ignition was uniform throughout the cross section of the propellant. The vessel was then pressurized with nitrogen, and the exhaust valve was kept open slightly to purge the combustion products.

A 10 A current was supplied to the electrodes connected from a DC power supply at 15 V to ignite the propellant sample. The video camera recorded the burning of the propellant through the window. Because the sample length was known, it was possible to obtain the burn rate of the propellant by replaying the recorded video frame by frame, where one frame corresponded to 0.04 s. Figure 3 shows the images of the burning propellant.

The residue in the window bomb experiments is defined as the percentage of the solid left unburned (that does not undergo gasification and is left over in the solid phase itself) to the initial weight of the propellant sample.

C. Burn Rate Results

Among the four propellant mixes made, as shown in Table 2, only mix 3 and mix 4 had residue of 10–13%; all other mixes resulted in higher residue of the order of 18%. Though the residue of 18% was marginally less than reported by Nanda and Ramakrishna [8] of

Table 2 Chemical composition of propellants tested

Mix	AP, wt %	IO, wt %	AC, wt %	Moisture, wt %	PTFE, wt %	Al, wt %	Binder, wt %	Residue, wt %	Density, kg/m^3
1	30	— —	— —	— —	1.765	10	58.235	18	1190
2	29.73	0.27	— —	— —	— —	10	60	18	1224
3	29.73	0.27	— —	— —	1.765	10	58.235	10-13	1212
4	29.7	— —	0.3	0.12	1.765	10	58.115	10-13	1162

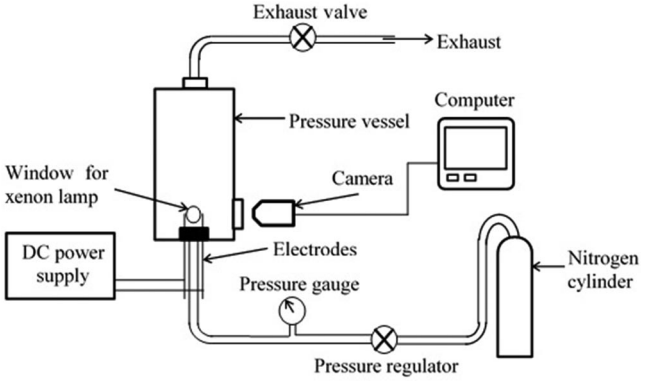

Fig. 2 Schematic of window bomb.

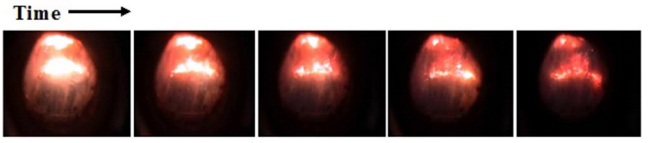

Fig. 3 Burning propellant sample images.

around 20–25%, it was considered high, and hence not considered for burn rate tests.

It can be seen in Table 2 that the addition of mechanically activated aluminum in mix 3 reduces the residue to 10–13% from 18% in mix 2, where only aluminum is used. This reaffirms the fact that mechanical activation of aluminum with PTFE increases its reactivity, as reported by Sipple et al. [15,16] and Gaurav and Ramakrishna [18]. As stated by Sipple et al. [15,16], the thermite reaction of aluminum and PTFE results in fluorination of aluminum which releases more energy than oxidation [15]. This could be taking place close to the propellant burning surface, and hence result in a large heat feedback to the propellant leading to lower residue. Also, the product of the aluminum PTFE reaction is aluminum fluoride, which sublimates at around 1500 K [16], unlike aluminum oxide, which tends to agglomerate and has a high boiling point of 3800 K [7].

Also, when AP embedded with AC and moisture absorbed in AC pores is used along with mechanically activated aluminum in mix 4, it reduces the residue to 10–13% from 18%, where only AP with mechanically activated aluminum is used in mix 1. This is similar to what is observed between mix 1 and mix 3, where IO embedded AP along with mechanically activated aluminum results in a lower residue of 10–13%.

A very interesting aspect that comes out of this study is that, when mechanically activated aluminum and catalyst embedded AP (be it AC or IO) are used together, the residue can be reduced up to 10–13%. If either one is used independently, the residues are higher (18%). This was something that Nanda and Ramakrishna [8] had not explored in their studies.

Burn rates measured for mix 3 and 4 are shown in Fig. 4a. Mix 4 exhibits a higher burn rate pressure index of 0.82, which is quite high to be used in a rocket motor due to fears of stability associated with combustion. The reason for this higher-pressure index with mix 4 had been discussed earlier in conjunction with the work done by Ishitha and Ramakrishna [19], where they had reported a higher-pressure index due to moisture presence in AC pores. The burn rate pressure index of 0.67 observed in the case of mix 3 is reasonably good. The highest burn rate recorded was 2 mm/s for mix 3 at 50 bar. The uncertainty in the measurement of the burn rate is around 6.5%.

As seen from Table 2, the residue of all propellant discussed is 10% or higher, which makes them unsuitable for any practical application. To further reduce the residue, it was thought to increase the solid loading by increasing the aluminum and AP content. This is similar to the boron-based FRP prepared by Kubota et al. [5]. The composition of this is shown in the Table 3.

Increasing the solid loading of the propellant not only resulted in an increase in propellant density but removed residue completely. The burn rates for this propellant are as shown in Fig. 4b. The burn rates obtained were higher than those achieved with lower solid loading propellants (mixes 3 and 4). The point shown on the burn rate curve in Fig. 4b will be discussed later. As this propellant yielded zero residue, accompanied by high burn rates and high densities, this was chosen as the candidate propellant for all further calculations for a hypersonic ramjet.

III. Comparison of Various Fuels Using Equilibrium Calculations

From Kubota et al.'s [5] work, it is evident that the temperatures achieved in the combustion chamber are quite high. To determine the temperatures associated with aluminum-based propellants and compare them with those of kerosene or hydrogen fuel, a series of calculations were made using the CEA code [21]. These calculations were carried out for an altitude of 37 km. The Mach number at the inlet of the combustor was held constant at 0.3 for all fuels. The ratio of specific heats γ for air was taken as a function of temperature as given in [22]. Figure 5 shows the maximum equilibrium combustion temperature of hydrogen, kerosene, and aluminum-based FRP (shown in Table 3) along with air stagnation temperature for different Mach numbers. The composition of mix 5 is similar to the typical boron-based FRP presented by Kubota et al. [5], except that boron is replaced with aluminum. It is seen that both kerosene and hydrogen have comparable maximum equilibrium combustion temperatures, whereas aluminum-based FRP has a maximum equilibrium temperature, which is consistently higher by around 250 K over kerosene and hydrogen at all Mach numbers. The temperature difference at Mach 5.5 with aluminum-based FRP between the stagnation temperature and the maximum possible combustion temperature at that particular Mach number is around 1500 K. This is similar to the temperature difference obtained with kerosene or

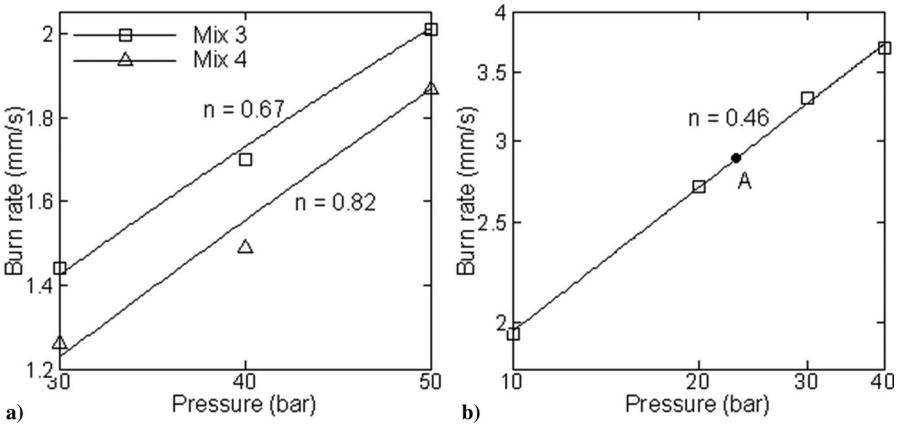

Fig. 4 Burn rate versus pressure for a) mixes 3 and 4 and b) aluminum FRP.

Table 3 Chemical composition of aluminum-based FRP

Mix	AP, wt %	Al, wt %	Binder, wt %	Density, kg/m^3
5	35	30	35	1528

hydrogen at a lower Mach number of around four. Therefore, it could be argued that, with aluminum-based FRP, the Mach number envelope of ramjets can be extended due to the higher combustion temperatures achieved with them.

Figure 6 shows the equilibrium combustion temperature for kerosene and aluminum-based FRP with air-fuel (A/F) ratio for Mach 6 at 25 km. Kerosene delivers the highest temperature at an A/F ratio of around 13, whereas aluminum-based FRP has its peak temperature at a much lower A/F ratio of four. This is a significant result that demonstrates that, for kerosene, if the A/F ratio is reduced below 13, the chamber temperature obtained drops, and hence the thrust also drops. However, for aluminum-based FRP, the A/F ratio can be reduced up to four and the temperatures are still higher than those obtained with kerosene. If both aluminum-based FRP and kerosene are used at the highest-temperature A/F ratios, the aluminum-based FRP will have 46% lower I_{sp} at an A/F ratio of four as compared to an A/F ratio of 13 for kerosene. The highest temperature at a lower A/F ratio of four in the case of aluminum-based FRP is due to the presence of oxidizer (AP) and aluminum itself, which has its stoichiometric A/F ratio of four with air. However, the advantage with aluminum-based FRP is the higher thrust and density as compared to kerosene as will be discussed later. Therefore, much higher thrust levels are possible with aluminum-based FRP; as the air–fuel ratio is small, the intake and vehicle size could be made smaller to reduce the drag.

Figure 7 shows the schematic of a ramjet with fuel-rich propellant. The ramjet design proposed here has two combustion chambers. The fuel-rich propellant burns in the primary combustor and ejects fuel-rich gases through a choked nozzle, as shown in Fig. 7, which burns completely with air in the secondary combustor and provides thrust. The pressure in the primary chamber is independent of the pressure in the secondary chamber, the flight altitude, and the Mach number. It depends only on the burn rate law of the propellant and the nozzle diameter. In this study, the intake is considered as a black box, and the pressure recovery and coefficient of drag are taken by extrapolating the experimental results reported by Dutton and Goldsmith [10]. As discussed earlier, a higher-equilibrium combustion temperature with aluminum-based FRP at a lower A/F ratio as compared to kerosene is achievable. In addition, with a nose cone mounted intake, a lower coefficient of drag is achievable as compared to a side-mounted intake. Hence, a much higher flight Mach number could be possible with this kind of intake and fuel combination.

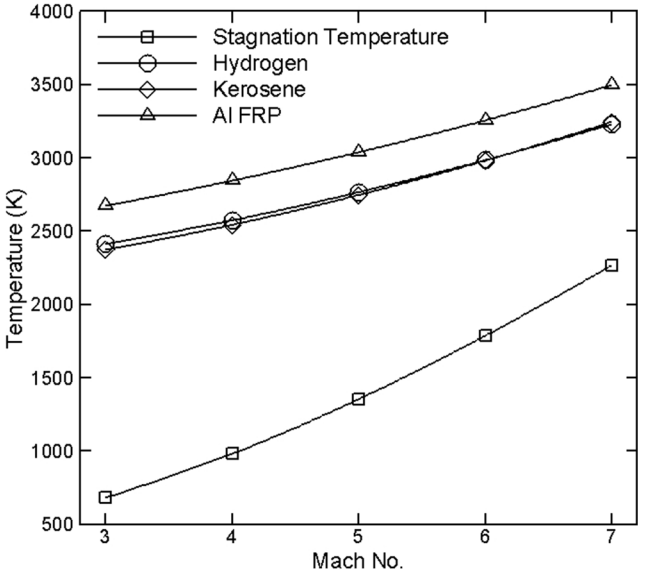

Fig. 5 Highest possible equilibrium combustion temperature of various fuels with Mach number.

IV. Mathematical Formulation

In this paper, a nondimensional thrust and drag analysis, which is independent of the system size, will be presented. The nondimensional thrust analysis was identical to the one presented by Mukunda [23]. A similar analysis has also been carried by Mattingly [24]. With this analysis, the required air–fuel ratio for a Mach 6 cruise flight can be obtained. For a level flight, thrust must overcome drag. In this analysis, efficiencies are absorbed in the pressure ratios. Temperature ratios are treated as those for an isentropic process. Flow through the nozzle is assumed to be optimally expanded.

A. Nondimensional Thrust Equation

Thrust generated by a ramjet is given by

$$F = \dot{m}_a\left[\left(1+\frac{1}{\epsilon}\right)v_4 - v_o\right] \tag{1}$$

where $\dot{m}_a$ is the air flow rate; ϵ is the air–fuel ratio; and v_4 and v_o are exit velocity of the gases through the nozzle and vehicle flight velocity, respectively. Nondimensionalizing the thrust with $\dot{m}_a a_o$ and writing v_4 and v_o in terms of the Mach number and temperature gives

$$\frac{F}{\dot{m}_a a_o} = M_o\left[\left(1+\frac{1}{\epsilon}\right)\frac{M_4}{M_o}\sqrt{\frac{T_4}{T_o}} - 1\right] \tag{2}$$

Here, it is assumed that the specific heat ratios and specific gas constant are same for both air and combustion products. To obtain

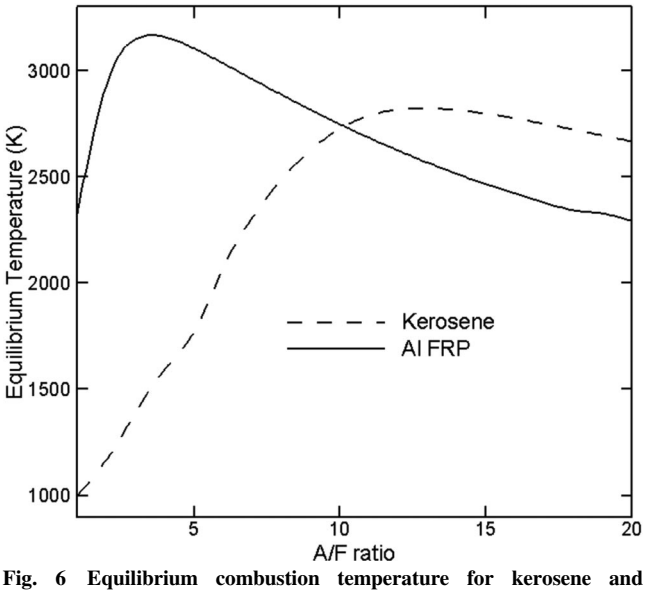

Fig. 6 Equilibrium combustion temperature for kerosene and aluminum FRP for Mach 6 at 25 km.

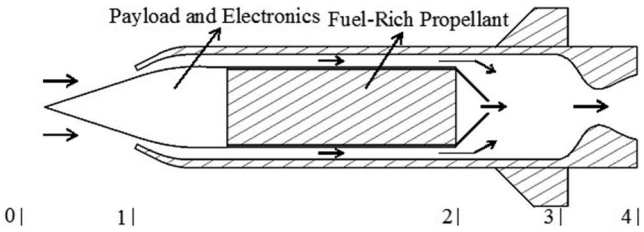

Fig. 7 Schematic of a ramjet with various station points.

T_4/T_o, temperature cascading has been performed. T_4/T_o can be expressed as

$$\frac{T_4}{T_o} = \frac{T_4}{T_{t4}}\frac{T_{t4}}{T_{t3}}\frac{T_{t3}}{T_o} \tag{3}$$

$$\frac{T_4}{T_o} = \frac{1}{(1+((\gamma-1)/2)M_4^2)}1\theta_b \tag{4}$$

where θ_b is the ratio of the chamber temperature to the ambient air static temperature. The subscript "t" in the temperature and pressure indicates the stagnation value, and the numbers correspond to the state from Fig. 7. The flow in the intake, burner and nozzle is assumed to be isentropic; therefore, the total temperature ratios for them are taken as unity.

Similarly, on doing pressure cascading, P_4/P_o can be expressed as

$$\frac{P_4}{P_o} = \frac{P_4}{P_{t4}}\frac{P_{t4}}{P_{t3}}\frac{P_{t3}}{P_{t2}}\frac{P_{t2}}{P_{t1}}\frac{P_{t1}}{P_{to}}\frac{P_{to}}{P_o} \tag{5}$$

As stated earlier, because the flow is optimally expanded, $P_4 = P_o$. The stagnation pressure ratios across the nozzle, burner, and diffuser are denoted with their corresponding pressure efficiencies as

$$\frac{P_{t4}}{P_{t3}} = \eta_n, \qquad \frac{P_{t3}}{P_{t2}} = \eta_b, \quad \text{and} \quad \frac{P_{t2}}{P_{to}} = \eta_d$$

respectively. Equation (5) can be written as

$$1 = \frac{1}{(1+((\gamma-1)/2)M_4^2)^{\gamma/(\gamma-1)}}\eta_n\eta_b\eta_d\left(1+\frac{\gamma-1}{2}M_o^2\right)^{\gamma/(\gamma-1)} \tag{6}$$

The diffuser efficiency is identical to the pressure recovery discussed in the literature on high-speed flows. Note that η_n, η_b, and η_d can be written as

$$\eta = (\eta_d\eta_b\eta_n)^{(\gamma-1)/\gamma} \tag{7}$$

Substituting this in Eq. (6), one gets

$$\left(1+\frac{\gamma-1}{2}M_4^2\right) = \eta\left(1+\frac{\gamma-1}{2}M_o^2\right) \tag{8}$$

Because

$$\theta_o = 1+\frac{\gamma-1}{2}M_o^2 \tag{9}$$

The ratio of M_4/M_o can be obtained using Eqs. (8) and (9). Substituting M_4/M_o and Eq. (4) in Eq. (2) will result in the following nondimensional thrust equation:

$$\frac{F}{\dot{m}_a a_o} = M_o\left[\left(1+\frac{1}{\epsilon}\right)\sqrt{\frac{\theta_b}{\eta\theta_o}\frac{(\eta\theta_o-1)}{\theta_o-1}}-1\right] \tag{10}$$

It can be seen from Eq. (10) that it depends only on the air–fuel ratio, flight Mach number, combustion chamber temperature, and overall efficiency, which includes the pressure efficiencies of the diffuser, burner and nozzle. An interesting aspect emerging out of this analysis is that the dependence of the thrust on the diffuser efficiency or pressure recovery is not large. Keeping the nozzle and burner pressure efficiency constant and taking a higher diffuser efficiency of three ramp intakes [3] and a lower diffuser efficiency of one ramp (based on [10]) for Mach 6, it is seen that, for a specific heat ratio (γ) of 1.4, even by reducing the diffuser efficiency by around three times, the overall efficiency reduces by only 30%.

Other than the aforementioned efficiencies, there is combustion efficiency that implicitly comes in the nondimensional thrust equation [Eq. (10)]. Combustion efficiency is defined as the ratio of measured characteristic exhaust velocity to theoretical characteristic exhaust velocity, which is expressed as

$$\eta_{c^*} = \frac{c^*_{\text{measured}}}{c^*_{\text{theoretical}}} \tag{11}$$

If the combustion efficiency is not 100%. then the combustion temperature that is used to obtain the θ_b value will not be the same as that calculated from the CEA code [21]. The characteristic exhaust velocity is a function of the square root of the combustion temperature; therefore, to calculate the actual temperature, the efficiency is to be squared. To account for combustion efficiency, θ_b is rewritten as θ'_b, which is defined as

$$\theta'_b = \theta_b\eta^2_{c^*} \tag{12}$$

Therefore, the nondimensional thrust can now be rewritten as

$$\frac{F}{\dot{m}_a a_o} = M_o\left[\left(1+\frac{1}{\epsilon}\right)\sqrt{\frac{\theta'_b}{\eta\theta_o}\frac{(\eta\theta_o-1)}{\theta_o-1}}-1\right] \tag{13}$$

Table 4 summarizes the effect of efficiencies on the nondimensional thrust for the $M = 6$ condition at an A/F ratio of 13 for aluminum-based FRP. It is seen that the nondimensional thrust drops by only 2% when the diffuser efficiency is lowered by 10%, whereas it drops by 50% when the combustion efficiency is reduced by 10%. Therefore, the nondimensional thrust has a higher sensitivity to combustion efficiency than the diffuser efficiency. The fact that the thrust generated is a function of both the combustion and diffuser efficiency was discussed earlier; however, the preceding calculation clarifies that the combustion efficiency plays a more pivotal role than the diffuser efficiency.

B. Nondimensional Drag Equation

The drag acting on the vehicle is given by

$$D = \frac{1}{2}\rho A v_o^2 c_d \tag{14}$$

Similar to thrust, nondimensionalizing the drag by $\dot{m}_a a_o$ will give

$$\frac{D}{\dot{m}_a a_o} = \frac{(1/2)\rho A v_o^2 c_d}{\dot{m}_a a_o} = \frac{(1/2)\rho A v_o^2 c_d}{\rho A_i v_o a_o} \tag{15}$$

Upon simplification, the nondimensional drag is given by the following equation:

$$\frac{D}{\dot{m}_a a_o} = \frac{1}{2}\frac{A}{A_i}M_o c_d \tag{16}$$

where A_i/A is the ratio of the air intake area to the vehicle frontal area. The aforementioned nondimensional drag equation comes out in an elegant form, and the number of variables is reduced by one from the drag equation. It has a linear dependence on the flight Mach number, the coefficient of drag, and the ratio of the air intake area to the vehicle frontal area.

Table 4 Sensitivity of nondimensional thrust with respect to other efficiencies

η_n, %	η_b, %	η_d, %	η_{c^*}, %	$F/\dot{m}_a a_o$
98	95	31	95	1.505
98	95	27.9	95	1.48
98	95	31	85.5	0.754

C. Ramjet Specific Impulse Equation

Equilibrium calculations were carried out using the CEA code [21]. The I_{sp} obtained from these calculations for different air–fuel ratios assumes that the air is carried on board the system as an oxidizer. Also, the ramjet takes in the incoming air as oxidizer, and therefore air comes into the engine with a certain momentum that needs to be considered, as proposed by Kubota and Kuwahara [25]. Along with the preceding, the combustion and thrust coefficient efficiencies are added here to make the calculations more realistic. The thrust coefficient efficiency, also known as the correction factor, accounts for the loss of thrust in the nozzle due to side thrust at the nozzle exit. This is seen in Eq. (17), which is an expression for the theoretical specific impulse of a ramjet:

$$I_{\text{sp\_ram}} = [(1+\epsilon)\eta_{c^*} \times \eta_{C_F} \times I_{\text{sp\_CEA}} - \epsilon v_o]/g \qquad (17)$$

V. Choice of Parameters

The nondimensional thrust and drag analyses were carried at two different altitudes of 18 and 25 km for three types of nose cone mounted intake pressure recovery. These included a three ramp and two ramp intakes from Hill and Peterson [3], as well as the experimental intake data given by Dutton and Goldsmith [10]. As stated earlier, in these analyses, the intake is treated as a black box and only the value of pressure recovery is considered here. Experimental data from Dutton and Goldsmith [10] for pressure recovery were taken for a 12 deg wedge intake, for which the results were available for only three Mach numbers of 1.56, 1.86, and 2.14. The pressure recoveries at all other Mach numbers were extrapolated from the data available, assuming an exponential decay with Mach number, and are shown in Fig. 8. For the other two intakes (namely, three ramps and two ramp intakes taken from Hill and Peterson [3]), a similar exercise of extrapolation was carried out beyond Mach 5. The pressure recovery variations with a Mach number for the three intakes considered in this study are shown in Fig. 8. As the single ramp intake based on [10] is the worst-case scenario for which experimental data are available only up to a Mach number of 2.14, a case study was carried out wherein the pressure recovery was further reduced by 30%. This is shown in Fig. 8 for a Mach number range from two to seven.

Experimental values for the coefficient of drag were taken from Dutton and Goldsmith [10], which were available only at three Mach numbers of 1.56, 1.86, and 2.14. They were extrapolated for the higher Mach numbers. The c_d values reported in [10] were for a model with no control and lifting surfaces, whereas the current system being contemplated would be one designed for cruise, and hence would have control and lifting surfaces. To account for this, a 20% higher coefficient of drag was considered over those reported in [10]. Figure 9 shows the coefficient of drag versus the Mach number used for calculations in this study. These are based on values reported in [10] along with 20 and 40% higher values. The 40% curve was included to account for the worst-case scenario possible, as the experimental data reported in [10] were only up to a Mach number of 2.14. The coefficient of drag variation with Mach number was assumed to be the same for all altitudes. Kubota et al. [5] reported that, for ramjets with boron-based FRP, the highest achievable combustion efficiency was 91%. Because aluminum is comparatively easier to burn, a combustion efficiency of 95% is assumed for aluminum-based FRP. The flow in the nozzle is assumed to be optimally expanded for all conditions. The other efficiencies and assumptions made for the calculations are shown in Table 5.

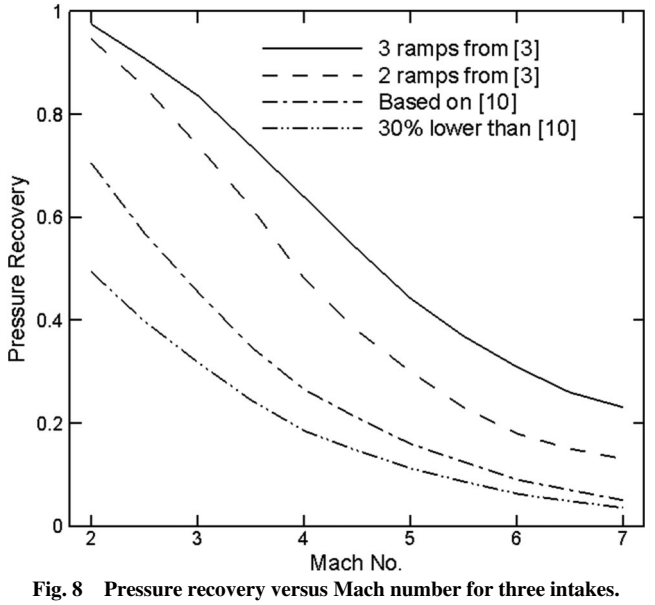

Fig. 8 Pressure recovery versus Mach number for three intakes.

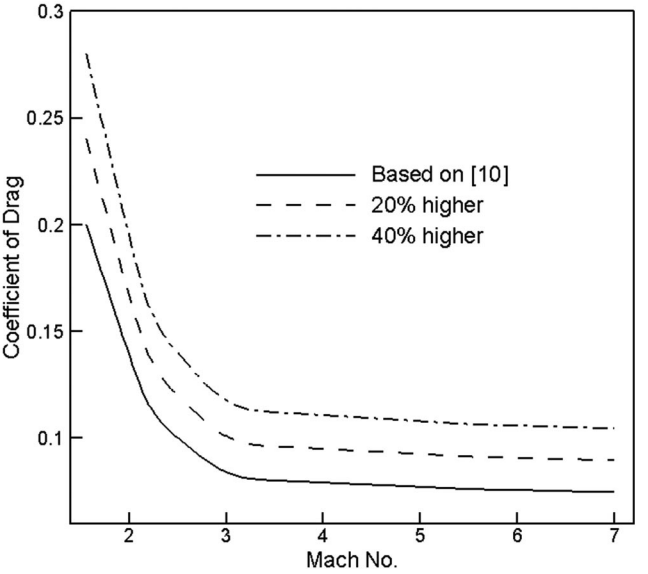

Fig. 9 Coefficient of drag versus Mach number for the intake based on [10].

VI. Results and Discussions

A. Nondimensional Thrust and Drag Analysis

Nondimensional thrust and drag and $I_{\text{sp\_ram}}$ calculations with Mach number were calculated based on Eqs. (13), (16), and (17) for two altitudes of 18 and 25 km with three kinds of air intake, as discussed earlier. The nondimensional thrust and drag curve shows the variation of thrust and drag with Mach number, and the crossover point at which the thrust and drag lines cross each other for a particular Mach number shows the A/F ratio required for a sustained flight at that Mach number. The vehicle can be operated at any other air–fuel ratio curve above this crossover curve. It would not be possible to operate it at any an air–fuel ratio curve below this because the thrust produced is not enough to counter the drag experienced by the vehicle. For a Mach 6 flight application, the crossover point was taken at a Mach number between 6 and 6.5 to be on a conservative side. Figure 10a shows the nondimensional thrust and drag curves for intake based on [10] at 25 km with 95% combustion efficiency.

The drag lines shown in the Fig. 10 were with a coefficient of drag being 20 and 40% higher than the base value already shown in Fig. 9. If a flight Mach number of six is chosen as the Mach number for level cruise flight, then Fig. 10a indicates the A/F ratio (crossover point) required for the flight. It is seen from Fig. 10a that, for a one ramp intake (based on [10]), the crossover point is at A/F ratio of 15; whereas for a three-ramp intake, which has the highest pressure recovery, this increases to 19. Further calculations will be presented with the intake based on [10], as this was the worst-case scenario with the lowest-pressure recovery factor.

A similar set of calculations was carried out for an altitude of 18 km to understand the effect of altitude on the crossover A/F ratio.

Table 5 Efficiencies and assumptions used for the calculations

Parameters	Values
η_{c^*}	95%
η_b	95%
η_n	98%
η_{C_F}	98%
Diffuser temperature loss	5%
A_i/A	0.4

Figure 10b shows the nondimensional thrust and drag versus Mach number for intake based on [10]. It was observed that the A/F ratio increased from 15 to 17 for 18 km. As the altitude reduced from 25 to 18 km, the ambient temperature decreased while θ_b' increased. This was because θ_b' had an inverse dependence on ambient temperature, as θ_b' increased with altitude reduction, even though the combustion temperatures were almost the same. Due to this reason, there was an increase in nondimensional thrust when altitude reduced. Similar trends were observed for other intake geometries too. The dotted line for an A/F of 17 represents calculations with a 30% lower pressure recovery over the one reported in [10]. In terms of absolute numbers, the pressure recovery is just 6.3% at Mach 6, as seen in Fig. 8. Even with such a low value of pressure recovery, it seems that a hypersonic Mach number is possible with aluminum-based FRP with a nose-mounted intake geometry. There is a lingering doubt that with 40% higher drag and 30% lower intake pressure recovery, the crossover Mach number is seen to reduce from 6.2 to 5.7 (refer Fig. 10b). These will be addressed a little later in the paper.

The $I_{\text{sp\_ram}}$ variation with the A/F ratio for three different intakes at 25 km is shown in Fig. 11. The dotted line shows the $I_{\text{sp\_ram}}$ at 18 km with intake based on [10]. There is a common trend that is followed by all the curves. Initially, the $I_{\text{sp\_ram}}$ increases with an increase in the A/F ratio; then, beyond a particular A/F ratio, it starts to drop. The reason for this trend can be understood from Eq. (17). As the A/F ratio increases, the exit velocity or the $I_{\text{sp\_CEA}}$ in Eq. (17) keeps on decreasing because the combustion temperature falls with increase in A/F ratio (refer Fig. 6). At a particular A/F ratio due to the effect of combustion efficiency and thrust coefficient efficiency, the exit velocity drops rapidly and the intake velocity (the term to the right of the negative sign in Eq. (17)) takes over, thereby reducing the $I_{\text{sp\_ram}}$ after that point. At 25 km altitude with the intake based on [10], the maximum A/F ratio at which it can operate is 15, as seen from Fig. 10, whereas the maximum $I_{\text{sp\_ram}}$ for this is achieved at an A/F ratio of eight; beyond this A/F ratio, $I_{\text{sp\_ram}}$ decreases, as seen in Fig. 11. Therefore, even though the flight can be operational at a higher A/F ratio of 15, it needs to be operated at an A/F ratio of eight to achieve the maximum $I_{\text{sp\_ram}}$. This accounts for the other aspect discussed in conjunction with Fig. 10b: namely, with the drop in intake pressure recovery and increase in drag, the crossover Mach number is seen to decrease. Similar trends were noticed for both two-ramp and three-ramp intakes, as seen from Fig. 11. The thrust line for these A/F ratios is above the crossover line; therefore, these are possible A/F ratios for a Mach 6 flight. This is fundamental result because it allows the intake area to be smaller with the FRP, hence making the overall vehicle dimensions smaller. This has been described as one major advantage of fuel-rich propellants by Mukunda [23].

Figure 12 is a condensed form of Fig. 11, wherein it shows the A/F ratio for the maximum $I_{\text{sp\_ram}}$ that can be achieved at 18 and 25 km for three intakes. It can be seen from Fig. 12 that, by improving the intake pressure recovery from an intake based on [10] to a three-ramp intake, $I_{\text{sp\_ram}}$ can be increased by more than 150 s at 25 km. The $I_{\text{sp\_ram}}$ at 18 km was slightly more than that at 25 km for the [10] intake; but, still, 25 km was chosen as the cruise altitude for Mach 6. Also, it was found that the intake area that was required to ingest sufficient air at 25 km was just 6% more than that required at 18 km. This increase in intake area was very nominal as compared to the 2.9 times lower drag at 25 km, which would mean a much lower fuel requirement and would pay off more than the higher $I_{\text{sp\_ram}}$ at 18 km for a system as a whole. In addition to this, the dynamic load on the vehicle will be less at 25 km as compared to the value at 18 km.

One more aspect that needs to be addressed is the problem of heating of the secondary combustion chamber for a hypersonic ramjet. The temperature of the compressed air that enters the combustor is around 1500 K. One may think that the temperatures at the end of combustion for a hypersonic ramjet will be much higher than a traditional ramjet and the insulation might fail to maintain its integrity. This paper proposes to use aluminum-based FRP ramjet at an A/F ratio of 5.5, which is the stoichiometric A/F ratio (refer Fig. 13), even though the highest $I_{\text{sp\_ram}}$ is achieved at an A/F ratio of

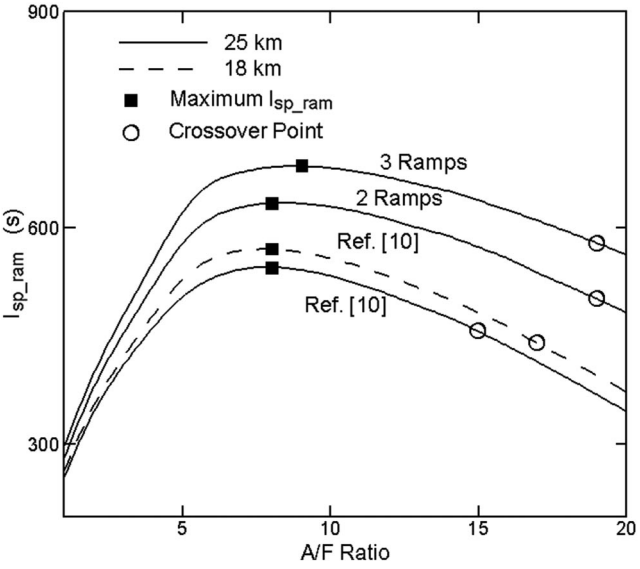

Fig. 11 $I_{\text{sp\_ram}}$ versus A/F ratio for three intakes at 18 and 25 km.

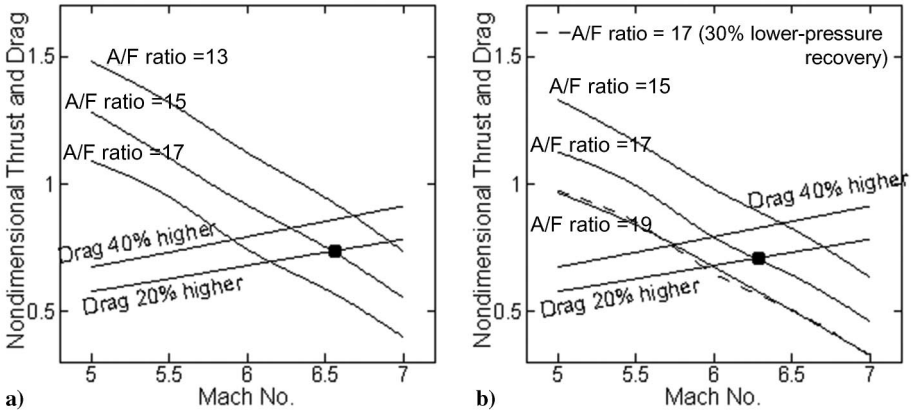

Fig. 10 Nondimensional thrust and drag versus Mach number with 95% combustion efficiency for intake based on [10] at a) 25 km and b) 18 km.

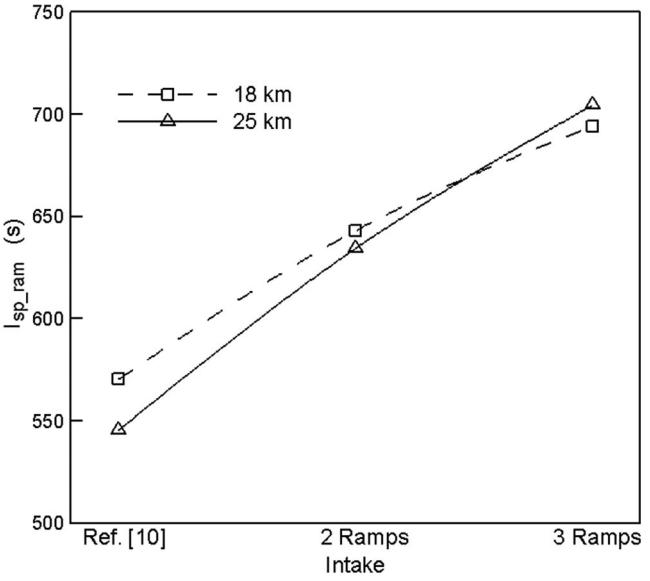

Fig. 12 Maximum I_{sp_ram} for three different intakes at 18 and 25 km.

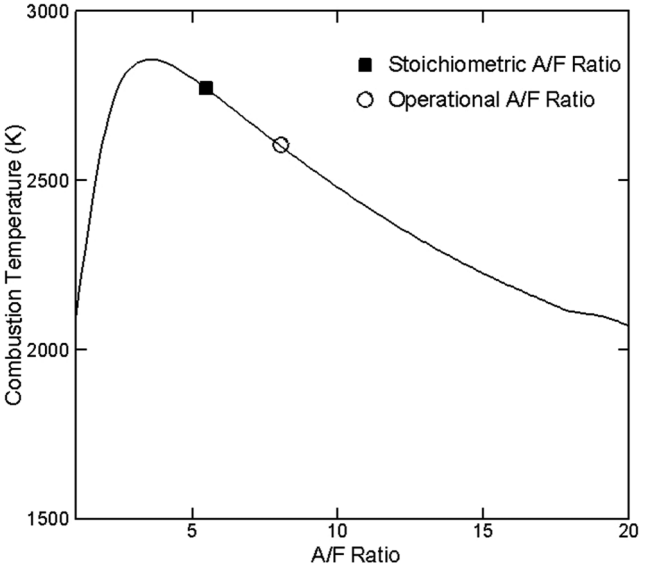

Fig. 13 Combustion temperature for aluminum FRP with 95% combustion efficiency for intake based on [10].

eight (refer Fig. 11). By doing so, there will be a marginal loss of 25 s in I_{sp_ram}, as is evident from Fig. 11. However, operating it at a stoichiometric A/F ratio will lead to low oxygen content in the gases flowing through the nozzle, and thus eliminates the oxidation of the nozzle and inhibitor. The nozzle erosion due to high aluminum content in the propellant is of concern in the primary combustion chamber. Typically, for an uncooled nozzle, the throat area is increased by around 6%, which results in a 6% decrease in chamber pressure [26]. The actual nozzle erosion rate for the designed propellant has to be determined experimentally. For the secondary chamber nozzle, this might not be significant due to the reduction in the aluminum/alumina content as the fuel-rich gases are getting mixed with air (discussed in the following).

In addition to the nozzle erosion issue, two phase losses occurring with regard to metallized propellant also need to be addressed. The aluminum content of 30% by weight in the FRP might seem to be very high compared to a typical solid propellant, where the aluminum content is 18% by weight. However, being a ramjet that is proposed to be operated at an A/F ratio of 5.5, the content of aluminum would only be around 5% by weight. It has been reported by Sutton and Biblarz [26] that the loss in I_{sp} due to two-phase flow is often less than 2% for a particle mass fraction of less than 6%. Thus, the two-phase losses will be minimal and most likely be lower than that with solid rockets.

In the literature [27] to evaluate thrust and drag for a hypersonic flight, a factor known as the thrust margin is often used. The thrust margin (TM) is the difference of thrust and drag over thrust. If the TM is greater than zero, the vehicle accelerates, i.e., the thrust is higher than drag. If the TM is lower than zero, the vehicle decelerates. In this paper, the TM is defined based on nondimensional thrust and drag, as shown in the following equation:

$$\mathrm{TM} = \frac{(F/\dot{m}_a a_o) - (D/\dot{m}_a a_o)}{F/\dot{m}_a a_o} \tag{18}$$

Table 6 shows the thrust margin at an A/F of 5.5 for the three intakes at 95% combustion efficiency. It is seen that there is a large thrust margin available and the vehicle can accelerate to higher Mach numbers. To have a cruise flight at Mach 6 with an A/F of 5.5, the airflow rate through the intake will have to be reduced, which will make the intake smaller.

B. Comparison with Kerosene and Hydrogen Scramjet

For a kerosene fueled scramjet, Dharavath et al. [28] reported a I_{sp} of 940 s using computational fluid dynamics simulations, whereas Zimont and Muhin [29] reported a I_{sp} of 450 s from theoretical calculations. The I_{sp} for a kerosene fuel-based scramjet could be in between these two values for an actual system. Zimont and Muhin [29] also carried out theoretical calculations for a hydrogen fuel-based scramjet and reported a maximum I_{sp} of around 1500 s. The aluminum-based FRP ramjet with 95% combustion efficiency can deliver a I_{sp_ram} close to 515 and 640 s at an A/F ratio of 5.5 with intake based on [10] and a three-ramp intake, respectively, for Mach 6 cruise at 25 km, as seen from Fig. 11. These values look very small in comparison to values of I_{sp} reported in the literature [28,29] with a kerosene or hydrogen-based scramjet engine. It needs to be explained how the FRP-based ramjet operating at hypersonic Mach numbers could be better than scramjets.

Any aerospace vehicle is always limited by volume. The range of the vehicle depends on the amount of fuel that can be stored in a given volume. That being the case, one has to look at the density of the fuel in order to make a comparison across different fuels.

To compare the kerosene and hydrogen fuel-based scramjet with the aluminum-based FRP ramjet, the aluminum-based FRP density specific impulse was normalized with the density of kerosene/hydrogen using Eq. (19). When this is done one, get the I_{sp} at either kerosene or hydrogen density:

$$(I_{sp\_ram})_{\mathrm{Kerosene/Hydrogen}} = \frac{(I_{sp\_ram} \times \mathrm{Density})_{\mathrm{AluminumFRP}}}{(\mathrm{Density})_{\mathrm{Kerosene/Hydrogen}}} \tag{19}$$

To evaluate the density of aluminum-based FRP, see the following equation:

$$\rho_p = \frac{1}{(m_{\mathrm{Al}}/\rho_{\mathrm{Al}}) + (m_{\mathrm{AP}}/\rho_{\mathrm{AP}}) + (m_{\mathrm{Binder}}/\rho_{\mathrm{Binder}})} \tag{20}$$

where m_{Al}, m_{AP}, and m_{Binder} are the mass fraction of aluminum, AP and the binder that, for the composition, are 0.3, 0.35, and 0.35, respectively. Note that ρ_{Al}, ρ_{AP}, and ρ_{Binder} are the density of the aluminum, AP and binder, which are 2700, 1950, and 962 kg/m^3,

Table 6 Thrust margin for aluminum FRP at A/F ratio of 5.5 with 95% combustion efficiency for three intakes

	TM
Intake based on [10]	0.723
Two-ramp intake	0.757
Three-ramp intake	0.767

Table 7 Specific impulse for aluminum FRP at its density and at the densities of kerosene and hydrogen

	Intake based on [10]	Three-ramp intake
I_{sp_ram} (in s), $\rho_{AluminumFRP} = 1528$ kg/m^3	515	640
$(I_{sp\_ram})_{Kerosene}$ (in s), $\rho_{Kerosene} = 810$ kg/m^3	971	1,207
$(I_{sp\_ram})_{Hydrogen}$ (in s), $\rho_{Hydrogen} = 70$ kg/m^3	11,241	13,970

respectively. With this expression and the individual ingredient densities as mentioned previously, the aluminum-based FRP density is 1528 kg/m^3.

Table 7 shows the specific impulse of aluminum-based FRP at the densities of kerosene and hydrogen. Even by considering a higher value of I_{sp} for a kerosene fuel-based scramjet as reported by Dharavath et al. [28], the aluminum-based FRP ramjet with [10] intake is better by just 3% but, with a three-ramp air intake, it is 28% better than a kerosene fuel-based scramjet. In comparison to a hydrogen fuel-based scramjet, the aluminum-based FRP ramjet is better by a factor of 7.5 due to the extremely low density of hydrogen. These I_{sp} values reaffirm the point that was made earlier in this paper regarding the advantage of density leading to higher volumetric heat release, as was explained in conjunction with Fig. 1.

C. System Calculations

All calculations presented in this paper up to this point are nondimensional in nature. In the initial part of the paper (Sec. II), an aluminum-based FRP (mix 5) was chosen as the candidate propellant because it had zero residue. To determine the burn rate requirement with aluminum-based FRP (mix 5) for a Mach 6 flight, a system size has to be chosen. Here, a vehicle diameter of 0.6 m is chosen and the coefficient of drag considered is 40% more than the baseline case. The thrust required to cruise at an altitude of 25 km is 2140 N. Accounting for wall thickness for the primary chamber casing, vehicle wall thickness, insulation thickness, and the gap for inlet air, the available diameter for the aluminum FRP has been assumed as 0.35 m. This accounts for a reasonable flight time of 200 s, and hence insulation thicknesses need to be large. For a I_{sp_ram} of 515 s (refer Table 7) and a density of 1528 kg/m^3 (refer Table 3), the required burn rate is around 2.9 mm/s for an end burning grain of 0.35 m in diameter. It can be seen from Fig. 4b that the required burn rate of 2.9 mm/s can be achieved at around a pressure of 23 bar (point A in Fig. 4b). Therefore, it can be safely concluded that, from a system point of view, aluminum-based FRP can deliver the required burn rates, and hence the performance for a Mach 6 cruise flight.

VII. Conclusions

Detailed calculations were carried out to come up with a ramjet system powered with fuel-rich propellant (FRP) that can be operated at hypersonic speeds. A nondimensional thrust and drag analysis was carried out, which was independent of the system size. Equilibrium calculations indicated that the aluminum-based FRP with its metal content could lead to a higher-equilibrium combustion temperature at a lower A/F ratio over kerosene, which could enhance the ramjet Mach number to six. Through a thorough nondimensional cycle analysis, it was shown that the thrust had a higher dependence on combustion efficiency than on the pressure recovery. It was found that, even with a low intake pressure recovery of around 9%, Mach 6 flight was possible. The specific impulse achieved for this condition was 515 s. A perturbation analysis was carried out on both the pressure recovery and coefficient of drag based on the values extrapolated from the literature. Even after reducing the pressure recovery by 30% to a value as low as 6.3% for Mach 6 and increasing the coefficient of drag by 40%, the aluminum-based FRP produced sufficient thrust for a sustained Mach 6 flight with a specific impulse of around 515 s. Also, operation of the ramjet at 25 km instead of 18 km, where the highest I_{sp_ram} was achieved, increased the air inlet area by just 6% but reduced the drag by 2.9 times, thereby lowering the fuel requirement. A comparison with a kerosene-based scramjet showed that aluminum-based FRP, from being nominally better, could be superior than the kerosene-fueled scramjet in terms of overall performance, depending on the intake pressure recovery achieved. However, over a hydrogen-fueled scramjet, it was more than seven times better due to its much higher density. However, all these nondimensional analyses are futile if an aluminized fuel-rich propellant cannot be developed to meet the thrust requirements. Therefore, with the use of various burn rate enhancement methods as reported in the literature, an aluminum-based FRP of higher density and zero residue was developed that also resulted in higher burn rates. Considering a system size, thrust requirements were arrived at based on the coefficient of drag and vehicle area for a Mach 6 flight at 25 km. The burn rate required of the FRP at these conditions was 2.9 mm/s. The aluminized FRP developed was able to achieve this burn rate at 23 bar. The aluminized FRP will burn at 23 bar in the primary chamber to supply the desired amount of fuel-rich gases to the secondary chamber, where they will react completely with air to provide thrust sufficient enough to sustain a level cruise flight of Mach 6 at 25 km. Thus, this paper has achieved its purpose of proposing a new design of a ramjet system with an appropriate fuel and showing through detailed calculations that a hypersonic system looks possible with a ramjet using a nose-mounted intake. However, designing such an intake that can provide higher-pressure recovery is still a challenge.

References

[1] Curran, E. T., "Scramjet Engines: The First Forty Years," *Journal of Propulsion and Power*, Vol. 17, No. 6, 2001, pp. 1138–1148. doi:10.2514/2.5875

[2] Tang, M., and Chase, R. L., "The Quest for Hypersonic Flight with Air-Breathing Propulsion," *15th AIAA International Space Planes and Hypersonic Systems and Technologies Conference*, AIAA Paper 2008-2546, 2008. doi:10.2514/6.2008-2546

[3] Hill, P., and Peterson, C., *Mechanics and Thermodynamics of Propulsion*, 2nd ed., Addison-Wesley, Lebanon, IN, 1992, pp. 20–22, 236–238.

[4] Gany, A, "Accomplishments and Challenges in Solid Fuel Ramjets and Scramjets," *International Journal of Energetic Materials and Chemical Propulsion*, Vol. 8, No. 5, 2009, pp. 421–446. doi:10.1615/IntJEnergeticMaterialsChemProp.v8.i5

[5] Kubota, N., Miyata, K., Kuwahara, T., Mitsuno, M., and Nakagawa, I., "Energetic Solid Fuels for Ducted Rockets (III)," *Propellants, Explosives, Pyrotechnics*, Vol. 17, No. 6, 1992, pp. 303–306. doi:10.1002/(ISSN)1521-4087

[6] Risha, G. A., Evans, B. J., Boyer, E., and Kuo, K. K., "Metals, Energetic Additives and Special Binders Used in Solid Fuels for Hybrid Rockets," *Fundamentals of Hybrid Rocket Combustion and Propulsion*, Vol. 218, Progress in Astronautics and Aeronautics, edited by Chiaverini, M. J., and Kuo, K. K., AIAA, Reston, VA, 2007, Chap. 10.

[7] Athawale, B. K., Asthana, S. N., and Singh, H., "Metallised Fuel-Rich Propellants for Solid Rocket Ramjet—A Review," *Defence Science Journal*, Vol. 44, No. 4, 1994, pp. 269–278. doi:10.14429/dsj.44.4182

[8] Nanda, J. K., and Ramakrishna, P. A., "Development of AP/HTPB Based Fuel-Rich Propellant for Solid Propellant Ramjet," *49th AIAA/ASME/SAE/ASEE Joint Propulsion Conference and Exhibit (JPC)*, AIAA Paper 2013-4171, 2013.

[9] Murty, M. S. R. C., and Chakraborty, D., "Coupled External and Internal Flow Simulation of a Liquid Fuelled Ramjet Vehicle," *Aerospace Science and Technology*, Vol. 36, July 2014, pp. 1–4. doi:10.1016/j.ast.2014.03.011

[10] Dutton, R. A., and Goldsmith, E. L., "The Drag of Some Wedge Centre-Body Intakes at Mach Numbers of 1.56, 1.86 and 2.14," British

Aeronautical Research Council, National Physical Lab., CP 968, 1966, Teddington, England, U.K., 1967.

[11] Gany, A., and Netzer, A. W., "Combustion Studies of Metallized Fuels for Solid-Fuel Ramjets," *Journal of Propulsion and Power*, Vol. 2, No. 5, 1986, pp. 423–427. doi:10.2514/3.22924

[12] Natan, B., and Gany, A., "Combustion Characteristics of a Boron-Fueled Solid Fuel Ramjet with Aft-Burner," *Journal of Propulsion and Power*, Vol. 9, No. 5, 1993, pp. 694–701. doi:10.2514/3.23677

[13] Kohga, M., "Burning Characteristics and Thermochemical Behavior of AP/HTPB Composite Propellant Using Coarse and Fine AP Particles," *Propellants, Explosives, Pyrotechnics*, Vol. 36, No. 1, 2011, pp. 57–64. doi:10.1002/prep.200900088

[14] Dokhan, A., Price, E. W., Seitzman, J. M., and Sigman, R. K., "The Effects of Bimodal Aluminum with Ultrafine Aluminum on the Burning Rates of Solid Propellants," *Proceedings of the Combustion Institute*, Vol. 29, No. 2, 2002, pp. 2939–2946. doi:10.1016/S1540-7489(02)80359-5

[15] Sippel, T. R., Son, S. F., and Groven, L. J., "Altering Reactivity of Aluminum with Selective Inclusion of Polytetrafluoroethylene Through Mechanical Activation," *Propellants, Explosives, Pyrotechnics*, Vol. 38, No. 2, 2013, pp. 286–295. doi:10.1002/prep.v38.2

[16] Sippel, T. R., Son, S. F., and Groven, L. J., "Aluminum Agglomeration Reduction in a Composite Propellant Using Tailored Al/PTFE Particles," *Combustion and Flame*, Vol. 161, No. 1, 2014, pp. 311–321. doi:10.1016/j.combustflame.2013.08.009

[17] Verma, S., and Ramakrishna, P. A., "Effect of Specific Surface Area of Aluminum on Composite Solid Propellant Burning," *Journal of Propulsion and Power*, Vol. 29, No. 5, 2013, pp. 1200–1206. doi:10.2514/1.B34772

[18] Gaurav, M., and Ramakrishna, P. A., "Effect of Mechanical Activation of High Specific Surface Area Aluminium with PTFE on Composite Solid Propellant," *Combustion and Flame*, Vol. 166, April 2016, pp. 203–215. doi:10.1016/j.combustflame.2016.01.019

[19] Ishitha, K., and Ramakrishna, P. A., "Activated Charcoal: As Burn Rate Modifier and Its Mechanism of Action in Nonmetalized Composite Solid Propellants," *International Journal of Advances in Engineering Sciences and Applied Mathematics*, Vol. 6, No. 1, 2014, pp. 76–96. doi:10.1007/s12572-014-0112-z

[20] Marothiya, G., and Ramakrishna, P. A., "A New and Effective Method to Enhance the Burn Rate of Composite Solid Propellants," *9th Asia-Pacific Conference on Combustion*, Combustion Inst. Korean Section, Gyeongju, ROK, 2013.

[21] Gordon, S., and McBride, B. J., "Computer Program for Calculation of Complex Chemical Equilibrium Compositions, Rocket Performance, Incident and Reflected Shocks, and Chapman-Jouguet Detonations," NASA SP-273, 1971.

[22] Hirschel, E. H., and Weiland, C., *Selected Aerothermodynamic Design Problems of Hypersonic Flight Vehicles*, Springer–Verlag, Berlin, 2009, Appendix B.

[23] Mukunda, H. S., *Understanding Aerospace Chemical Propulsion*, Interline Publishing, Bangalore, India, 2004, pp. 42–46, 111–121.

[24] Mattingly, J. D., *Elements of Propulsion: Gas Turbines and Rockets*, AIAA Educational Series, AIAA, Reston, VA, 2006, pp. 266–272.

[25] Kubota, N., and Kuwahara, T., "Combustion of Energetic Fuel for Ducted Rockets (I)," *Propellants, Explosives, Pyrotechnics*, Vol. 16, No. 2, 1991, pp. 51–54. doi:10.1002/(ISSN)1521-4087

[26] Sutton, G. P., and Biblarz, O., *Rocket Propulsion Elements*, 7th ed., Wiley, New York, 2001, pp. 88–89.

[27] Curran, E. T., and Murthy, S. N. B., *Scramjet Propulsion*, Vol. 189, Progress in Astronautics and Aeronautics, AIAA, Reston, VA, 2000, pp. 386–388.

[28] Dharavath, M., Manna, P., and Chakraborty, D., "Computational Fluid Dynamics Simulation of Tip-to-Tail for Hypersonic Test Vehicle," *Journal of Propulsion and Power*, Vol. 31, No. 5, 2015, pp. 1370–1379. doi:10.2514/1.B35686

[29] Zimont, V. L., and Muhin, E. S., "Theoretical Maximum Efficiency and Specific Impulse of the External Burning Scramjet," *Journal of Propulsion and Power*, Vol. 29, No. 5, 2013, pp. 1031–1040. doi:10.2514/1.B34596

E. L. Petersen
Associate Editor